THE ASTROPHYSICAL JOURNAL, 436:818–830, 1994 December 1

THE EFFECTS OF GRAVITY DARKENING ON THE ULTRAVIOLET CONTINUUM POLARIZATION PRODUCED BY CIRCUMSTELLAR DISKS

J. E. BJORKMAN AND K. S. BJORKMAN
Department of Astronomy and Space Astronomy Laboratory, 425 N. Charter Street, University of Wisconsin, Madison, WI 53706
Received 1994 May 9; accepted 1994 June 6

ABSTRACT

We investigate the effects of gravity darkening on the UV continuum polarization produced by an axisymmetric disk that surrounds a rapidly rotating star. Although the model is a single scattering approximation, we do include the effects of attenuation (electron scattering plus hydrogen bound-free absorption) by the disk, using an approach similar to that of Sobolev (1963). Because of the gravity darkening of the star and the attenuation within the disk, the radiation field is not axially symmetric about the radius vector. This implies that the polarization source functions are no longer provided by the finite disk depolarization factors of Cassinelli, Nordsieck, & Murison (1987), which are functions of the intensity moments in a spherically symmetric atmosphere. We reformulate the polarization source functions using generalized intensity moment tensors (J, H_i, K_{ij}) that are valid for an arbitrary radiation field and envelope geometry. We find that the polarization source functions are simplest when using intensity moments in the observer's reference frame. On the other hand, the intensity moments are most easily evaluated in the stellar reference frame. Using the rotation transformation properties of the generalized intensity moments, we relate the observer's moments to those evaluated in the stellar reference frame. Our procedure for determining the polarization source functions thus merely involves choosing a set of Euler angles for the coordinate rotations, and then evaluating the associated rotation matrix. The geometrical complications of polarization transfer are thus reduced to obtaining a coordinate rotation matrix.

Using this method, we calculate the polarization produced by a circumstellar disk. Because the scattered radiation, which is dominated by light from the stellar equator, has a lower effective temperature than the direct radiation from the star, the polarization shortward of the Wien peak is smaller than previously expected. This UV depolarization is largest for rapid rotators, later spectral types, and envelope geometries that have a small density ratio between the equator and pole. We find that for a thin dense disk, the amount of UV depolarization is inadequate to explain the observed UV polarization of Be stars. Thus their UV depolarization is most likely a result of metal line blanketing by the envelope. For envelopes that are only moderately flattened, there is significant polarization cancellation by the polar material, owing to the polar brightening of the star, but the shape is incorrect to explain the UV observations of Be stars. In some instances gravity darkening causes the polar cancellation to be large enough that the position angle flips by 90°. Thus gravity darkening provides a new method for causing a wavelength-dependent position angle flip for a disk geometry, which is a possible polarization diagnostic for distinguishing thin dense disks from moderately flattened envelopes.

Subject headings: circumstellar matter — polarization — radiative transfer — scattering — stars: emission line, Be

1. INTRODUCTION

Be stars are rapidly rotating near-main-sequence stars that are believed to have equatorially concentrated circumstellar envelopes. They are generally variable at all wavelengths. Evidence from ultraviolet, optical, infrared, and radio observations has led to a picture of a dense equatorial disk geometry (for a recent review, see Waters 1994). Polarimetric observations support this view, showing definite signatures that are characteristic of an axisymmetric geometry (e.g., Coyne 1976; McLean & Clarke 1979). Because the polarized flux is attenuated by the envelope, polarization measurements provide a valuable probe of the distribution of density and temperature within the envelope.

Prior to the flight of the Wisconsin Ultraviolet Photo-Polarimeter Experiment (WUPPE) aboard Astro-1, only optical and infrared observations of the polarization of Be stars had been made. Prior to WUPPE, the standard models of UV polarization produced by a circumstellar envelope had predicted that Be stars should have a rising polarization toward shorter wavelengths in the UV (e.g., Poeckert & Marlborough 1978; Cassinelli, Nordsieck, & Murison 1987). These model predictions were based on the assumption that the polarization in Be stars is produced by electron scattering modified by the effects of hydrogen bound-free opacity. Optical polarization measurements had agreed with these model predictions quite well.

The results from WUPPE observations of the UV polarization of three Be stars were quite surprising, however. Figure 1 shows the polarization as a function of wavelength for the Be star ξ Tauri. The UV data are from WUPPE, and the optical data are contemporaneous observations made at the Pine Bluff Observatory (PBO) of the University of Wisconsin. Instead of rising into the UV, the polarization continuum remains relatively flat, and large regions of depolarization are observed near 1700 and 1900 Å (Bjorkman et al. 1991, 1993, hereafter Paper I and Paper II). In Papers I and II, several suggestions were made as to the cause of the discrepancies between the models and the observed UV continuum polarization. One suggestion is the effect of metal line blanket-

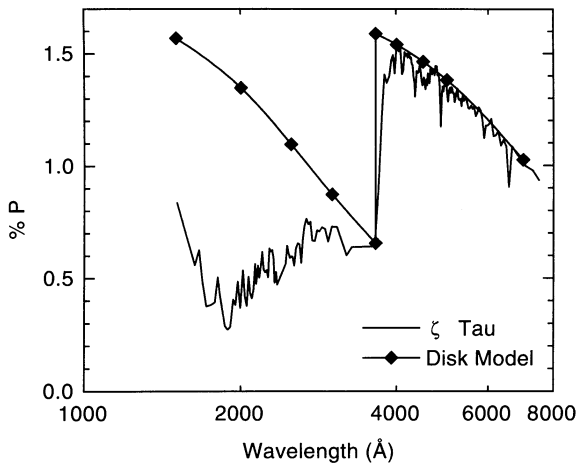

FIG. 1.—Observed polarization of ζ Tau (B1 IVe–sh) compared with a theoretical disk model. The UV data were obtained by the Wisconsin Ultraviolet Photo-Polarimeter Experiment (WUPPE) and the optical data were obtained at the University of Wisconsin Pine Bluff Observatory (PBO). The model calculations are for an equatorial disk and include hydrogen bound-free absorption, which is responsible for the wavelength dependence of the polarization. Note the large disagreement in the UV.

ing of the polarized flux by the circumstellar envelope. That effect is not the subject of this paper. Another possibility, the effect of gravity darkening, was proposed because Be stars are rapid rotators. The rapid rotation, as a result of the von Zeipel (1924) effect, decreases the effective temperature of the equatorial regions of the star (gravity darkening). This leads to temperature differences between the flux scattered in the disk and the unscattered flux coming directly from the star, as pointed out in Paper I. Note that this effect is due to scattering by the disk, and is not the same as the polarization produced by scattering in the photosphere of a rotating star (Collins 1970; Collins, Truax, & Cranmer 1991).

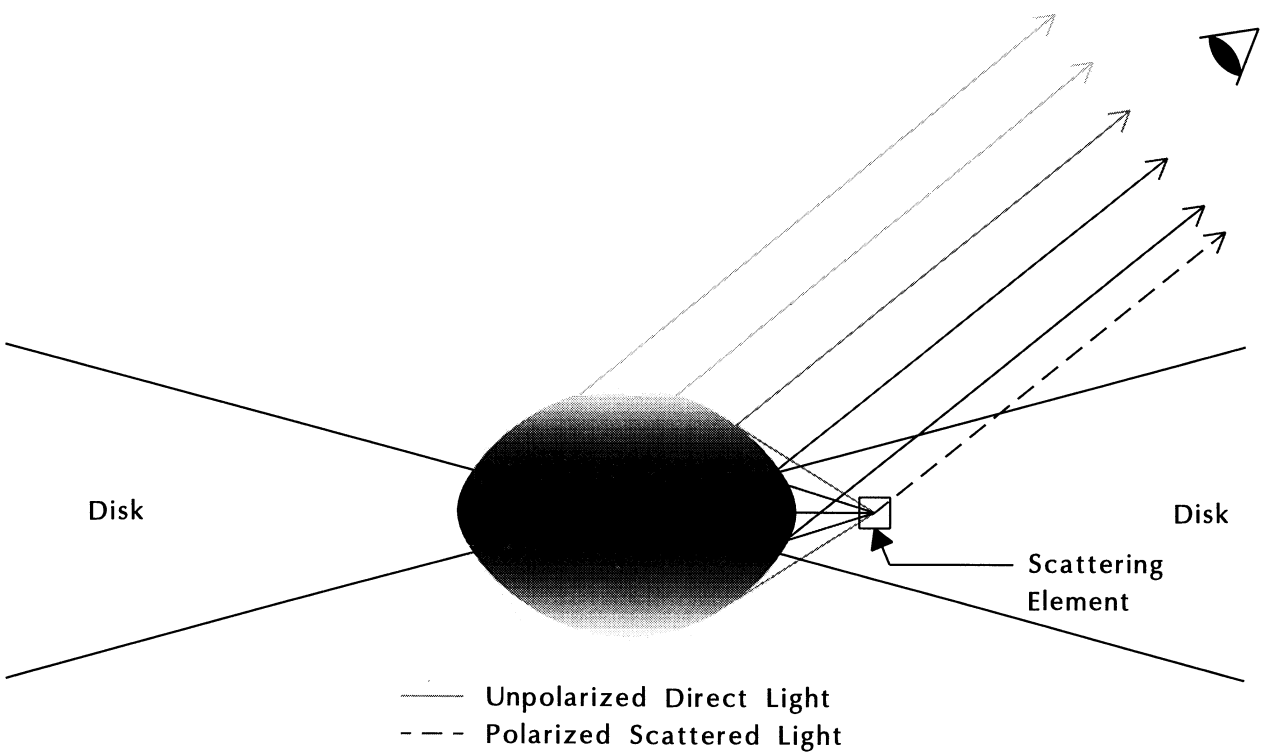

FIG. 2.—Schematic diagram that illustrates how the scattered polarized radiation (*dashed line*) can have a lower radiation temperature than the direct radiation from the star (*solid lines*). Shown is a star rotating at 90% of break-up, which is flattened as a result of the rotation. The shading is an indication of the effective temperature. The cooler equatorial region is dark and the hotter polar region is light. Surrounding the star is a circumstellar disk, which contains free electrons that scatter the stellar radiation. Within the disk we have depicted an individual scattering volume element. Note as a result of the shape of the star that the scatterers cannot see the hot polar region (except at large radii where there is little contribution to the net polarization); therefore, the scattered radiation tends to be at a lower average radiation temperature than the light that is observed directly from the star.

The gravity darkening effects are largest at the equator and, as shown in Figure 2, the radiation scattered by the disk originates primarily in the equatorial regions of the star. Thus it has a lower average temperature, T_{sc}, than the average temperature, T_*, of the direct (unscattered) radiation from the inclined star. The direct radiation consists of an average over all latitudes of the star. But because of limb darkening, the average tends to be dominated by radiation from a colatitude equal to the inclination angle of the star, so $T_* \sim T_{\rm eff}(\theta = i)$. The polarization is given by the ratio of scattered flux to direct flux, so qualitatively we expect that

$$P \sim \frac{B_\nu^{sc}}{B_\nu^*} = \begin{cases} \dfrac{T_{sc}}{T_*} & \left(\nu \ll \dfrac{kT_{sc}}{h}\right); \\ \exp\left[\dfrac{h\nu}{k}\left(\dfrac{1}{T_{sc}} - \dfrac{1}{T_*}\right)\right] & \left(\nu \gg \dfrac{kT_*}{h}\right). \end{cases} \tag{1}$$

Redward of the Wien peak of the scattered radiation, this ratio is constant, so the polarization will be wavelength independent, except for the normal "saw-tooth" behavior produced by the hydrogen bound-free opacity. However, blueward of the Wien peak of the direct radiation, this ratio decreases exponentially. This will cause the polarization to decrease into the UV and will tend to offset the increase in polarization produced by the decreasing bound-free hydrogen opacity. The amount of gravity darkening depends on the rotation rate of the star, so the faster the star rotates the larger the UV polarization decrease.

Note that the temperature of the scattered and direct light from the star is actually an average over the stellar surface as seen by the scatterers and observer, respectively. This averaging tends to dilute the temperature difference. However, in the UV, limb darkening is quite pronounced, and will limit the range of latitudes that contribute to the average temperature. Thus limb darkening will tend to accentuate the temperature difference between the direct and scattered light, so it is important to include both limb and gravity darkening in the model. In this paper, we will examine in more detail the combined effects of both gravity and limb darkening on the polarization in the UV, and investigate to what extent this mechanism can explain the WUPPE observations of Be stars.

2. MODEL DEFINITION

There are several factors that we must consider when calculating the effects of gravity darkening on the UV polarization. First, the scattered and the direct flux both depend on integrations of the stellar intensity over the solid angle subtended by the star as seen by the scatterers and the observer, respectively. These integrations determine the average temperatures of the scattered and direct radiation, so to account for gravity darkening, we must treat the star as an extended source. Second, because of the potentially large increase in the low temperature equatorial surface area, it is important to account for the increase in equatorial radius associated with the rapid rotation. Close to the star, where most of the polarization is produced, this increase in radius helps shield the low-latitude scatterers from the hot polar radiation, thereby reducing the temperature of the scattered radiation. Third, as mentioned previously, limb darkening is quite pronounced in the UV and will also tend to shield the equatorial scatterers from the hot polar radiation. Finally, to test whether or not gravity darkening can explain the observed UV continuum polarization, we must include the large hydrogen bound-free opacity. Thus, our basic model consists of a rapidly rotating star, which is flattened due to the rotation. The effective temperature of the star is a function of latitude, and the intensity emitted from the surface includes the effects of limb darkening. Finally the star is surrounded by an axisymmetric disklike circumstellar envelope, which provides free electrons and hydrogen that attenuate both the direct and scattered light.

The effects of metal line opacities are also quite important in the UV, but since we wish to independently investigate the relative importance of gravity darkening versus line blanketing, we defer that (more complicated) analysis (see Wood & Bjorkman 1994 for some preliminary results on the effects of line attenuation within the disk).

2.1. *Coordinate Systems*

To perform the flux integrals that determine the intrinsic polarization, we must specify a coordinate system. We orient an observer's Cartesian coordinate system so that the star is at the origin, the observer is on the z-axis at $+\infty$, and the z-y plane contains the stellar rotation axis (see Fig. 3). In this coordinate system, the plane of the sky is the x-y plane. When integrating along various lines of sight toward the star, we employ a two-dimensional polar coordinate system on the sky, where q is the impact parameter of the line of sight and α is the "position angle" measured counterclockwise from the x-axis, thus

$$\begin{aligned} x &= q\cos\alpha\,, \\ y &= q\sin\alpha\,. \end{aligned} \tag{2}$$

We orient a stellar Cartesian coordinate system, denoted by a subscript $*$, with the z_*-axis along the stellar rotation axis, and the y_*-axis along the observer's x-axis. The transformation from the observer's coordinates to the stellar coordinates is obtained from a rotation about the x-axis by the inclination angle, i, of the star, which gives

$$\begin{aligned} x_* &= -q\sin\alpha\cos i + z\sin i\,, \\ y_* &= q\cos\alpha\,, \\ z_* &= q\sin\alpha\sin i + z\cos i\,. \end{aligned} \tag{3}$$

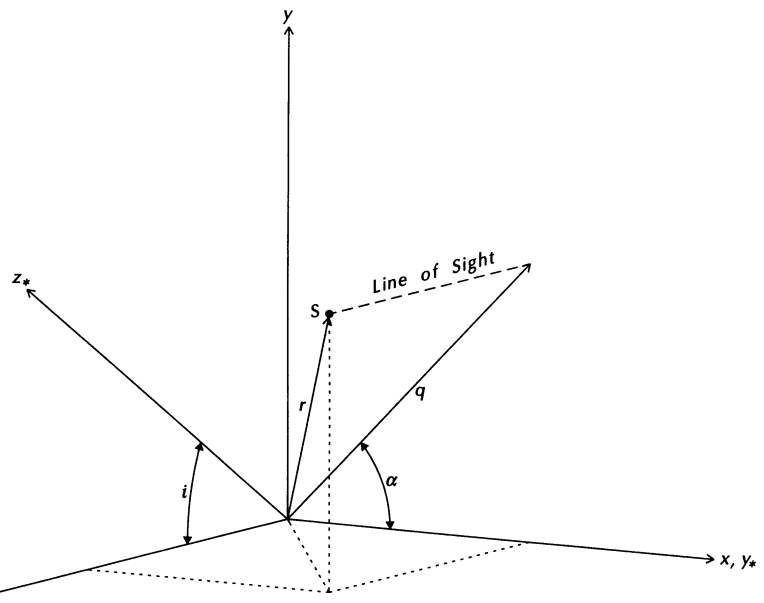

FIG. 3.—Orientation of the observer's and stellar coordinate systems. The observer is at $+\infty$ on the z-axis, the star is at the origin, and the stellar rotation axis, z_*, is inclined by an inclination angle, i. Shown is a line of sight with position angle, α, and impact parameter, q, that passes through the point S, where the star light is scattered.

Finally, since the density is given in spherical polar coordinates, we also need the transformation from the observer's coordinates to spherical polar stellar coordinates (r, θ, ϕ):

$$r^2 = q^2 + z^2 ,$$

$$\sin\theta = \left[\frac{q^2\cos^2\alpha + (q\sin\alpha\cos i - z\sin i)^2}{q^2 + z^2}\right]^{1/2} ,$$

$$\cos\theta = \frac{q\sin\alpha\sin i + z\cos i}{\sqrt{q^2 + z^2}} ,$$

$$\sin\phi = \frac{q\cos\alpha}{\sqrt{q^2\cos^2\alpha + (q\sin\alpha\cos i - z\sin i)^2}} ,$$

$$\cos\phi = \frac{-q\sin\alpha\cos i + z\sin i}{\sqrt{q^2\cos^2\alpha + (q\sin\alpha\cos i - z\sin i)^2}} . \tag{4}$$

Before determining the flux, we must first find the emergent intensities for each Stokes parameter, $\boldsymbol{I}_\nu^{\rm em} = (I_\nu, Q_\nu, U_\nu, V_\nu)|_{z=+\infty}$, as a function of line of sight impact parameter, q, and position angle, α.

2.2. *Polarization Source Functions*

We begin by considering a scattering volume element at the point S (see Figs. 3 and 4) with stellar coordinates (r, θ, ϕ) and electron number density n_e. We construct a local Cartesian coordinate system with its origin at the point S and with its x', y', and z' axes parallel to the $\hat\theta$, $\hat\phi$, and $\hat r$ directions, respectively. Next consider the specific intensity in the direction of the point P shown in Figure 4. Let θ' be the spherical polar angle of the direction P, measured from the $\hat r$-direction in the local coordinate system, and ϕ' be its azimuthal angle, measured from the $\hat\theta$-direction. The scattering contribution from integrating over all such directions to the specific intensity along the line of sight is (see Chandrasekhar 1960, pp. 34–40)

$$\frac{d\boldsymbol{I}_\nu}{dz} = \frac{n_e\sigma_{\rm T}}{4\pi}\int \boldsymbol{L}(\pi - \psi)\boldsymbol{R}(\chi)\boldsymbol{L}(-\psi')\boldsymbol{I}_\nu^{\rm inc}(\theta', \phi')d\Omega' , \tag{5}$$

where $\sigma_{\rm T}$ is the Thomson cross section, ψ and $(2\pi - \psi')$ are the position angle of the scattering plane in the reference frames of the observer and the star, respectively (see Fig. 4), $\boldsymbol{L}(\psi)$ is the transformation matrix for the Stokes parameters due to a clockwise rotation of the reference axes by the angle ψ, $\boldsymbol{R}(\chi)$ is the phase matrix for Rayleigh scattering by an angle χ, and $d\Omega' = \sin\theta'\, d\theta'\, d\phi'$.

If we assume that any incident radiation is unpolarized, so that $\boldsymbol{I}_\nu^{\rm inc} = (I_\nu^{\rm inc}, 0, 0, 0)$, then the transfer equation for the Stokes vector specific intensities is (see, e.g., Chandrasekhar 1960)

$$\frac{d}{dz}\boldsymbol{I}_\nu = -(\kappa_\nu\rho + n_e\sigma_{\rm T})\boldsymbol{I}_\nu + \left(\frac{3n_e\sigma_{\rm T}}{16\pi}\right)\int\begin{pmatrix} 1 + \cos^2\chi \\ -\cos(2\psi)\sin^2\chi \\ -\sin(2\psi)\sin^2\chi \\ 0 \end{pmatrix} I_\nu^{\rm inc}d\Omega' + \begin{pmatrix} j_\nu \\ 0 \\ 0 \\ 0 \end{pmatrix} , \tag{6}$$

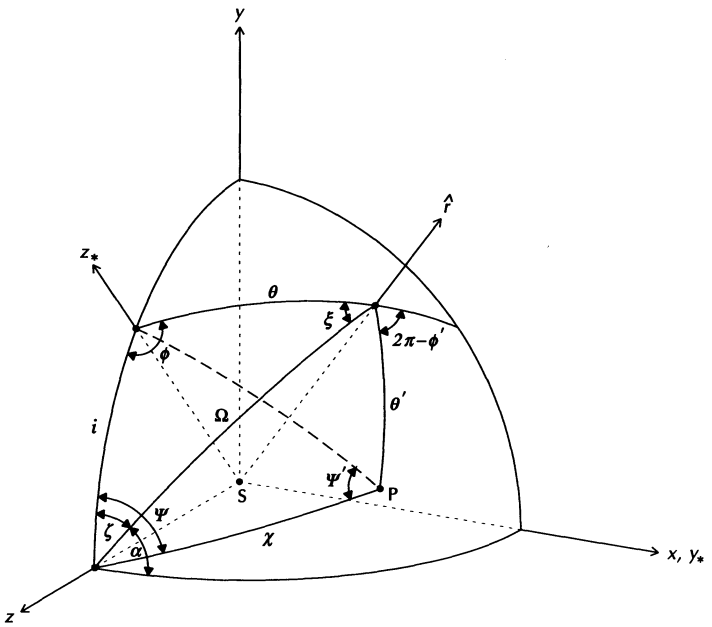

FIG. 4.—Scattering geometry. This figure shows the spherical triangles required to determine the angles between various directions at the scattering volume element, S, which has stellar coordinates (r, θ, ϕ). The direction away from the center of the star is shown by the unit vector, $\hat{r}$. Incident radiation in the direction, P, is scattered through an angle, χ, into the line of sight direction, z.

where ρ is the density, κ_ν is the absorptive opacity, and j_ν is any additional source of unpolarized continuum emission, such as free-free or free-bound emission. Instead of using θ' and ϕ' for the integration over all solid angles, we may instead use χ and ψ as the independent variables, in which case $d\Omega = \sin\chi\, d\chi\, d\psi$. To simplify the evaluation of the scattering integral, we introduce the generalized intensity moments (see, e.g., eqs. [1-4], [1-19], and [1-28] of Mihalas 1978, pp. 5–13)

$$J = \frac{1}{4\pi}\int I_\nu\, d\Omega\,,$$

$$H_i = \frac{1}{4\pi}\int I_\nu \hat{n}_i\, d\Omega\,, \tag{7}$$

$$K_{ij} = \frac{1}{4\pi}\int I_\nu \hat{n}_i \hat{n}_j\, d\Omega\,,$$

where

$$\begin{aligned} \hat{n}_z &= \cos\chi\,, \\ \hat{n}_x &= \sin\chi\cos(\pi/2-\psi)\,, \\ \hat{n}_y &= \sin\chi\sin(\pi/2-\psi)\,. \end{aligned} \tag{8}$$

Using the above definition of the intensity moments (7), the transfer equation (6) may be written as

$$\frac{d}{dz}\boldsymbol{I}_\nu = -(\kappa_\nu\rho + n_e\sigma_T)\boldsymbol{I}_\nu + \left(\frac{3n_e\sigma_T}{4}\right)\begin{pmatrix} J+K_{zz} \\ K_{xx}-K_{yy} \\ -2K_{xy} \\ 0 \end{pmatrix}_\nu + \begin{pmatrix} j_\nu \\ 0 \\ 0 \\ 0 \end{pmatrix}. \tag{9}$$

We define the polarization "source functions" to be

$$\boldsymbol{S}_\nu = \frac{3n_e\sigma_T}{4}\begin{pmatrix} J+K_{zz} \\ K_{xx}-K_{yy} \\ -2K_{xy} \\ 0 \end{pmatrix}_\nu + \begin{pmatrix} j_\nu \\ 0 \\ 0 \\ 0 \end{pmatrix}. \tag{10}$$

Note that we have not divided by the extinction coefficient, $k_\nu = \kappa_\nu\rho + n_e\sigma_T$; later it is more convenient to use z as the integration variable instead of the optical depth, τ_ν.

If we were to naively integrate the transfer equation (9) for a particular line of sight, we would evaluate the intensity moments at each point along the line of sight. In determining the flux, we would thus evaluate the intensity moments at each point in the three-dimensional volume (not occulted by the star). However, note that under coordinate rotations, the zeroth moment, J, transforms as a scalar, the first moment, $\boldsymbol{H}$, is a vector, and the components of $\boldsymbol{K}$ form a second-rank symmetric tensor. Consequently we may evaluate the intensity moments in a more convenient reference frame, such as the stellar frame, and then use the appropriate rotation matrix to obtain the intensity moments in the observer's coordinate system. Additionally we know that in the reference frame of the star, axisymmetry ensures that the intensity moments are functions only of r and θ. As a result, we can save an enormous amount of computation time by first evaluating the intensity moments in the stellar reference frame as a function of r and θ, and then when we integrate the transfer equation, we only need to transform these moments by the appropriate rotation matrix. To evaluate the moments at the scattering volume S, we use the local coordinate system with basis vectors $\hat{r}$, $\hat{\theta}$, and $\hat{\phi}$. In this coordinate system

$$J' = \frac{1}{4\pi}\int I_\nu \, d\Omega' ,$$
$$H'_i = \frac{1}{4\pi}\int I_\nu \hat{n}'_i \, d\Omega' , \tag{11}$$
$$K'_{ij} = \frac{1}{4\pi}\int I_\nu \hat{n}'_i \hat{n}'_j \, d\Omega' ,$$

and the unit vector, $\hat{n}'$, is

$$\hat{n}'_r = \cos\theta' ,$$
$$\hat{n}'_\theta = \sin\theta' \cos\phi' , \tag{12}$$
$$\hat{n}'_\phi = \sin\theta' \sin\phi' ,$$

where θ' is the polar angle measured from $\hat{r}$, ϕ' is the azimuth measured from $\hat{\theta}$, and $d\Omega' = \sin\theta' \, d\theta' \, d\phi'$.

To transform the intensity moments from the stellar coordinate system to the observer's coordinate system we must determine the rotation matrix, which requires that we specify three Euler angles. There are two different sets that prove convenient depending on the application. The first set of Euler angles consists of (θ, ϕ, i) shown in Figure 4. The resulting rotation matrix is

$$\boldsymbol{R} = \boldsymbol{R}_r(\pi/2)\boldsymbol{R}_\phi(i)\boldsymbol{R}_r(-\phi)\boldsymbol{R}_\phi(-\theta)$$
$$= \begin{pmatrix} \cos i \cos\theta + \sin i \sin\theta \cos\phi & -\cos i \sin\theta + \sin i \cos\theta \cos\phi & -\sin i \sin\phi \\ \sin\theta \sin\phi & \cos\theta \sin\phi & \cos\phi \\ \sin i \cos\theta - \cos i \sin\theta \cos\phi & -\sin i \sin\theta - \cos i \cos\theta \cos\phi & \cos i \sin\phi \end{pmatrix}, \tag{13}$$

where $\boldsymbol{R}_r$ denotes a rotation about the instantaneous $\hat{r}$-axis, and $\boldsymbol{R}_\phi$ denotes a rotation about the instantaneous $\hat{\phi}$-axis. Rows 1–3 correspond to z, x, and y, respectively, and columns 1–3 correspond to r, θ, and ϕ, respectively. The second set of Euler angles, also shown in Figure 4, is (ξ, Ω, ζ), which gives the alternate expression

$$\boldsymbol{R} = \boldsymbol{R}_r(\zeta - \pi/2)\boldsymbol{R}_\phi(-\Omega)\boldsymbol{R}_r(\xi)$$
$$= \begin{pmatrix} \cos\Omega & -\cos\xi \sin\Omega & -\sin\xi \sin\Omega \\ \sin\zeta \sin\Omega & \sin\xi \cos\zeta + \cos\xi \sin\zeta \cos\Omega & -\cos\xi \cos\zeta + \sin\xi \sin\zeta \cos\Omega \\ \cos\zeta \sin\Omega & -\sin\xi \sin\zeta + \cos\xi \cos\zeta \cos\Omega & \cos\xi \sin\zeta + \sin\xi \cos\zeta \cos\Omega \end{pmatrix}. \tag{14}$$

The transformation of J, $\boldsymbol{H}$, and $\boldsymbol{K}$ from stellar to observer's coordinates is now given by

$$J = J' ,$$
$$\boldsymbol{H} = \boldsymbol{R}\boldsymbol{H}' , \tag{15}$$
$$\boldsymbol{K} = \boldsymbol{R}\boldsymbol{K}'\boldsymbol{R}^T .$$

Note that because the polarization source functions (10) are simple functions of the observer's intensity moments, J and $\boldsymbol{K}$, all of the geometrical complexity of finding the polarization source functions is now confined to the well known procedure for determining a rotation matrix, $\boldsymbol{R}$.

2.2.1. *Axially Symmetric Radiation Field*

As a special case, if the radiation field is axially symmetric about the radius vector, $\hat{r}$, (as is the case for either plane parallel or spherically symmetric atmospheres), then

$$\boldsymbol{H}' = \begin{pmatrix} H_\nu \\ 0 \\ 0 \end{pmatrix}, \qquad \boldsymbol{K}' = \begin{pmatrix} K_\nu & 0 & 0 \\ 0 & \frac{1}{2}(J_\nu - K_\nu) & 0 \\ 0 & 0 & \frac{1}{2}(J_\nu - K_\nu) \end{pmatrix}, \tag{16}$$

where J_ν, H_ν, and K_ν are the usual intensity moments (i.e., in the radial direction). Inserting the intensity moments (16) into the transformation equation (15) yields

$$\boldsymbol{H} = H_\nu \begin{pmatrix} R_{zr} \\ R_{xr} \\ R_{yr} \end{pmatrix}, \qquad \boldsymbol{K} = \tfrac{1}{2}(J_\nu - K_\nu)\mathbf{1} + \tfrac{1}{2}(3K_\nu - J_\nu) \begin{pmatrix} R_{zr}^2 & R_{zr}R_{xr} & R_{zr}R_{yr} \\ R_{zr}R_{xr} & R_{xr}^2 & R_{xr}R_{yr} \\ R_{zr}R_{yr} & R_{xr}R_{yr} & R_{yr}^2 \end{pmatrix}, \tag{17}$$

where $\mathbf{1}$ is the identity matrix. Inserting these moments into the source functions (10) we find

$$\boldsymbol{S}_\nu = \left(\frac{3n_e\sigma_T}{8}\right) \begin{pmatrix} (3J_\nu - K_\nu) + (3K_\nu - J_\nu)R_{zr}^2 \\ (3K_\nu - J_\nu)(R_{xr}^2 - R_{yr}^2) \\ -2(3K_\nu - J_\nu)R_{xr}R_{yr} \\ 0 \end{pmatrix} + \begin{pmatrix} j_\nu \\ 0 \\ 0 \\ 0 \end{pmatrix}. \tag{18}$$

Using the rotation matrix with Euler angles (θ, ϕ, i), equation (13), we obtain the source functions in the stellar spherical polar coordinate system,

$$\boldsymbol{S}_\nu = \left(\frac{3n_e\sigma_T}{8}\right) \begin{pmatrix} (3J_\nu - K_\nu) + (3K_\nu - J_\nu)(\cos i\cos\theta + \sin i\sin\theta\cos\phi)^2 \\ (3K_\nu - J_\nu)[\sin^2\theta\sin^2\phi - (\sin i\cos\theta - \cos i\sin\theta\cos\phi)^2] \\ 2(3K_\nu - J_\nu)\sin\theta\sin\phi(\cos i\sin\theta\cos\phi - \sin i\cos\theta) \\ 0 \end{pmatrix} + \begin{pmatrix} j_\nu \\ 0 \\ 0 \\ 0 \end{pmatrix}. \tag{19}$$

Note that this equation agrees with equation (71) of Bjorkman (1992), and disagrees with I-component of equations (34)–(36) of Brown, Carlaw, & Cassinelli (1989) (to correct their formulae, one should set $f_S = 1$ in their eq. [36]). If instead we substitute the rotation matrix with Euler angles (ξ, Ω, ζ), equation (14), into equation (18), we find the source functions in the observer's coordinate system,

$$\boldsymbol{S}_\nu = \left(\frac{3n_e\sigma_T}{8}\right) \begin{pmatrix} (3J_\nu - K_\nu) + (3K_\nu - J_\nu)\cos^2\Omega \\ -(3K_\nu - J_\nu)\cos(2\zeta)\sin^2\Omega \\ -(3K_\nu - J_\nu)\sin(2\zeta)\sin^2\Omega \\ 0 \end{pmatrix} + \begin{pmatrix} j_\nu \\ 0 \\ 0 \\ 0 \end{pmatrix}, \tag{20}$$

which agrees with equations (2), (11), (12), and (16) of Cassinelli et al. (1987).

2.2.2. *Axisymmetric Density Distribution*

At any point in a general axisymmetric density distribution, the radiation field must be symmetric about the plane containing the radius vector and the stellar rotation axis, that is, $I_\nu(\theta', \phi') = I_\nu(\theta', -\phi')$. Since I_ν is even with respect to ϕ', we see from the moment definition, equations (11) and (12), that $H'_\phi = K'_{r\phi} = K'_{\theta\phi} = 0$. Using this result with equation (15) for the moment transformations and the fact that $K_{ij} = K_{ji}$, the source functions (10) simplify to

$$\boldsymbol{S}_\nu = \left(\frac{3n_e\sigma_T}{4}\right) \begin{pmatrix} J' + K'_{rr}R_{zr}^2 + K'_{\theta\theta}R_{z\theta}^2 + K'_{\phi\phi}R_{z\phi}^2 + 2K'_{r\theta}R_{zr}R_{z\theta} \\ K'_{rr}(R_{xr}^2 - R_{yr}^2) + K'_{\theta\theta}(R_{x\theta}^2 - R_{y\theta}^2) + K'_{\phi\phi}(R_{x\phi}^2 - R_{y\phi}^2) + 2K'_{r\theta}(R_{xr}R_{x\theta} - R_{yr}R_{y\theta}) \\ -2[K'_{rr}R_{xr}R_{yr} + K'_{\theta\theta}R_{x\theta}R_{y\theta} + K'_{\phi\phi}R_{x\phi}R_{y\phi} + K'_{r\theta}(R_{xr}R_{y\theta} + R_{x\theta}R_{yr})] \\ 0 \end{pmatrix} + \begin{pmatrix} j_\nu \\ 0 \\ 0 \\ 0 \end{pmatrix}. \tag{21}$$

This is the form of the source functions that we employ for our gravity darkening calculations.

2.3. *Geometry*

To evaluate the intensity moments that appear in the polarization source functions, we must specify the geometry of the stellar surface. We also require the density of the circumstellar envelope, because the stellar intensity is attenuated by the optical depth from scattering volume to the stellar surface.

2.3.1. *The Star*

We assume that the surface of the star is approximately given by an equipotential surface of the effective gravity,

$$\Phi_{\rm eff} = -\frac{GM(1-\Gamma)}{r} - \frac{1}{2}\omega^2 r^2 \sin^2\theta\,, \tag{22}$$

where $\Gamma = \sigma_e L/4\pi GcM$ is the ratio of radiative to gravitational acceleration, L is the stellar luminosity, σ_e is the electron scattering opacity per gram, ω is the angular rotation speed of the star, and we have assumed that most of the stellar mass, M, is distributed in a spherically symmetric core. Solving for the radius, we obtain

$$\frac{R(\theta)}{R_{\rm pole}} = \left[\sin\left\{\frac{1}{3}\sin^{-1}\left[\sin\theta\sin\left(3\sin^{-1}\frac{V_{\rm rot}}{2V_{\rm crit}}\right)\right]\right\}\right]\left\{\sin\theta\,\frac{V_{\rm rot}}{2V_{\rm crit}}\left[1 - \frac{1}{3}\left(\frac{V_{\rm rot}}{V_{\rm crit}}\right)^2\right]\right\}^{-1}, \tag{23}$$

where R_{pole} is the polar radius, V_{rot} is the equatorial rotation speed, and $V_{crit} \equiv [2GM(1 - \Gamma)/(3R_{pole})]^{1/2}$ is the critical or break-up velocity. Note that the equatorial radius is $R_{eq} = R_{pole}/[1 - \frac{1}{3}(V_{rot}/V_{crit})^2]$.

2.3.2. *The Envelope*

To motivate our parameterization of the density, we assume that the circumstellar envelope is produced by a stellar wind that travels outward with a "Beta velocity law,"

$$v_r = v_\infty\left(1 - 0.96\,\frac{R(\theta)}{r}\right)^\beta . \tag{24}$$

For the exponent we choose $\beta = 0.8$, which is the value obtained by Friend & Abbott (1986) in their study of radiatively-driven winds. We also assume that the wind has a larger mass flux at the equator than at the pole. Combining mass conservation with the velocity law, equation (24), we adopt the following parameterization of the wind density

$$n_e = n_0\,\frac{[1 + B\sin^m\theta]}{r^2[1 - 0.96R(\theta)/r]^\beta} . \tag{25}$$

Note that the parameter B controls the ratio of the polar to equatorial density, the parameter m controls the thickness of the disk, and the density scale, n_0, controls the optical depth of the envelope. The half width (in latitude) half maximum of the density distribution is $\Delta\theta = \cos^{-1}(2^{-1/m})$.

2.4. *Gravity and Limb Darkening*

In addition to the shape of the star, we also require the stellar intensity emitted from the surface as a function of position and direction. The von Zeipel theorem determines the radiative flux, H, or equivalently the effective temperature of the star, as a function of latitude

$$T_{eff} = T_{pole}(g_{eff}/g_{pole})^{1/4} , \tag{26}$$

where $g_{pole} = GM(1 - \Gamma)/R_{pole}^2$, and $g_{eff} = |-\nabla\Phi_{eff}|$ is the effective surface gravity of the star as a function of latitude. The polar temperature, T_{pole}, is determined by matching the total luminosity with the integral of the flux over the stellar surface.

For our limb darkening law, we use the Eddington-Barbier relation, which implies that at the stellar surface

$$I_\nu^*(\mu) = B_\nu\left[1 + \mu\,\frac{d\ln B_\nu}{d\tau}\right]\Bigg|_{\tau=0} , \tag{27}$$

where $\mu = \cos\theta'' = -\hat{n}'\cdot\hat{n}''$, and θ'' is the angle between the line of sight direction, $\hat{n}'$, and the unit normal to the stellar surface, $\hat{n}'' = \nabla\Phi_{eff}/g_{eff}$. We obtain the surface temperature from the gray atmosphere approximation, $B = 3H(\tau + \frac{2}{3})$, which implies that

$$T_0 \equiv T|_{\tau=0} = \left(\frac{1}{2}\right)^{1/4} T_{eff} , \qquad \frac{d\ln B_\nu}{d\tau}\Bigg|_{\tau=0} = \frac{3}{8}\left[\frac{h\nu/kT_0}{1 - \exp(-h\nu/kT_0)}\right] . \tag{28}$$

2.5. *Hydrogen Bound-Free Opacity*

When calculating the intensity moments in the envelope, the stellar intensities must be attenuated not only by electron scattering, but also by the large hydrogen opacity in the circumstellar disk. Similarly the radiation will sustain additional attenuation after it has been scattered. For the bound-free opacity, we assume that the ionization balance of hydrogen is primarily determined by photoionization and radiative recombination. Given these considerations, we parameterize the number of neutral hydrogen atoms in the $n = 2$ and 3 levels by

$$n_i^H = \frac{q_i n_e^2}{W} \qquad (i = 2, 3) , \tag{29}$$

where $W = 0.5\{1 - [1 - (r/R)^2]^{1/2}\}$ is the dilution factor. The proportionality constant, q_i, is determined by matching the average excitations, $\bar{q}_i \equiv \int_R^\infty n_i^H\,dr/\int_R^\infty n_e^2\,dr$, shown in Figure 3 of Cassinelli et al. (1987), which presents the results of a detailed non-LTE calculation. Using their density law, $q_i = 0.24\bar{q}_i$, so for a B2 star ($T_{eff} = 20{,}000$ K), we find $q_2 = 3.5 \times 10^{-21}$ cm^3 and $q_3 = 4.7 \times 10^{-22}$ cm^3.

In general the hydrogen ionization fraction coefficients, q_i, are functions of temperature. If we were to include the temperature dependence of the hydrogen ionization fraction, the size of the polarization Balmer jump would depend on spectral type. However, we wish to study the spectral type dependence of the gravity darkening effects for a fixed optical polarization level and polarization Balmer jump. We could adjust the envelope density and geometry to compensate for the changes in hydrogen bound-free opacity and maintain a constant optical polarization level and Balmer jump independent of spectral type. However, changing the envelope geometry complicates the interpretation of the results, so we have chosen instead to isolate the spectral type dependence by neglecting the temperature dependence of the hydrogen ionization fraction coefficients, q_i; instead we use the values above for a typical Be star.

In addition to hydrogen bound-free opacity, we also include free-free opacity, since free-free emission and absorption can be important at longer wavelengths. The total absorptive opacity is given by

$$\kappa_\nu\rho = a_{f-f}\left[1 - \exp\left(-\frac{h\nu}{kT}\right)\right]\frac{n_e^2}{\nu^3T^{1/2}} + \begin{cases} n_2\,a_2(\nu_2/\nu)^3 + n_3\,a_3(\nu_3/\nu)^3 & (\nu > \nu_2) , \\ n_3\,a_3(\nu_3/\nu)^3 & (\nu_2 > \nu > \nu_3) . \end{cases} \tag{30}$$

where the free-free absorption coefficient $a_{f-f} = 3.692 \times 10^8$ cm^5 s^{-3} K$^{1/2}$, and the photoionization cross sections $a_2 = 1.4 \times 10^{-17}$ cm^2 and $a_3 = 2.2 \times 10^{-17}$ cm^2 at the Balmer and Paschen thresholds, ν_2 and ν_3, respectively.

We must balance the absorption with unpolarized free-bound plus free-free emission. From equation (4.23) in Osterbrock (1989, pp. 86–90), the bound-free plus free-free emission is given by

$$j_\nu = \frac{1}{4\pi} \gamma_\nu(\mathrm{H}^0, T) n_e^2 . \tag{31}$$

The values of $\gamma_\nu(\mathrm{H}^0, T)$ are given in Table 4.7 in Osterbrock (1989) or may be calculated using his equations (4.21) and (4.22).

2.6. *Intensity Moments*

Given the stellar geometry and envelope opacities, we can now calculate the intensity moments in the envelope. We assume that the only contribution to the intensity moments J' and K'_{ij} is the direct light from the star attenuated by the optical depth, τ_1, between the stellar surface and the scattering volume (this is essentially the same approximation used by Sobolev 1963, pp. 119–120, to investigate the polarization of sunlight in the Earth's atmosphere). In this case

$$J' = \frac{1}{4\pi} \int_{\Omega_*} e^{-\tau_1} I_\nu^*(\mu)\, d\Omega' , \qquad K'_{ij} = \frac{1}{4\pi} \int_{\Omega_*} e^{-\tau_1} I_\nu^*(\mu) \hat{n}'_i \hat{n}'_j\, d\Omega' , \tag{32}$$

where Ω_* is the solid angle subtended by the star, and $\tau_1 = \int_0^{s_*} k_\nu\, ds$ is the optical depth to the stellar surface, which is at a distance s_* in the direction $\hat{n}'$ from the scattering volume. When integrating the intensity moments, first we numerically find the intersection point of the current line of sight with the stellar surface, which gives us the latitude and effective temperature of the star at that point. We next find the angle between the line of sight and the unit normal to the stellar surface, and finally, we calculate the optical depth to the stellar surface.

2.7. *Emergent Intensities*

Although the transfer equation (9) is valid for optically thick radiation transfer, we have not included any diffuse contribution (from other parts of the envelope) to the intensity moments (32). Similarly, we have not included any contribution to the source functions from polarized incident radiation; consequently, our model is effectively a *single scattering* approximation that includes a correction for optical depth effects (see Fox 1993 for a discussion of how to include the polarized contributions to the source functions, and see Hillier 1993 for a discussion of how to include the polarized diffuse radiation field). Note that since the line of sight attenuation includes electron scattering opacity, this correction does not properly conserve the number of photons. The advantage of not including any diffuse radiation is that the polarization source functions only depend on the stellar intensity moments, so we may use the formal solution to the transfer equation to calculate the emergent intensities. Thus,

$$\boldsymbol{I}_\nu^{\mathrm{em}}(q, \alpha) = \begin{cases} \int_{z_*}^{+\infty} e^{-\tau_2(z)} \boldsymbol{S}_\nu\, dz + e^{-\tau_2(z_*)} \boldsymbol{I}_\nu^*(\mu) & [q < q_*(\alpha)] , \\ \int_{-\infty}^{+\infty} e^{-\tau_2(z)} \boldsymbol{S}_\nu\, dz & [q > q_*(\alpha)] , \end{cases} \tag{33}$$

where the optical depth $\tau_2(z) = \int_z^{+\infty} k_\nu\, dz$, z_* is the location where the line of sight intersects the stellar surface, $\mu = \hat{z} \cdot \hat{n}''$, and $q_*(\alpha)$ is the impact parameter of the stellar limb at position angle α. Note that we have employed z as the integration variable instead of τ_2, because we do not a priori know the inversion $z(\tau_2)$, which would be required to evaluate the source functions. Consequently it is more convenient to use z as the integration variable, which is why, earlier, we defined our "source functions" without the usual division by the extinction coefficient, k_ν.

To solve the emergent intensity integrals (33), one could employ a simple quadrature routine that would numerically evaluate the optical depth, $\tau_2(z)$, for each point in the integrand. However, it is much more efficient to simultaneously solve for both the optical depth and the intensity by recasting the integrals in the form of the following set of simultaneous differential equations:

$$\frac{dt}{dz} = k_\nu t , \qquad \frac{d\boldsymbol{I}_\nu^{\mathrm{em}}}{dz} = -t \boldsymbol{S}_\nu , \tag{34}$$

where the attenuation factor $t = \exp(-\tau_2)$, and we use the initial values $t = 1$ and $\boldsymbol{I}_\nu^{\mathrm{em}} = 0$ at $z = +\infty$. If $q < q_*(\alpha)$ we integrate to $z = z_*$ and add $t\boldsymbol{I}_\nu^*(\mu)$, otherwise we integrate to $z = -\infty$.

2.8. *Flux Integration*

From the emergent intensities we find the total flux,

$$\boldsymbol{F}_\nu = \frac{1}{d^2} \int_0^{2\pi} d\alpha \int_0^{\infty} \boldsymbol{I}_\nu^{\mathrm{em}}(q, \alpha) q\, dq , \tag{35}$$

where d is the distance to the star. For an inclined axisymmetric envelope, the optical depth is left-right symmetric under reflections through the y-z plane; that is, $\tau_2(x, y, z) = \tau_2(-x, y, z)$. Under this transformation the I- and Q-components of $\boldsymbol{S}$ (see eq. [10]) are symmetric, but S_U is antisymmetric, because $K'_{xy}(x, y, z) = -K'_{xy}(-x, y, z)$. Consequently, U_ν^{em} is antisymmetric, so F_U vanishes. Thus the only nonzero components of the Stokes flux vector are

$$\begin{pmatrix} F_I \\ F_Q \end{pmatrix}_\nu = \frac{2}{d^2} \int_{-\pi/2}^{+\pi/2} d\alpha \int_0^{\infty} \begin{pmatrix} I_\nu^{\mathrm{em}} \\ Q_\nu^{\mathrm{em}} \end{pmatrix}_\nu q\, dq . \tag{36}$$

Note that because of the left-right symmetry, we only need to integrate over $x > 0$. Since $F_U = 0$, the net polarization is

$$P = \frac{F_Q}{F_I}, \tag{37}$$

and the position angle is a constant independent of wavelength (except for line effects where the Doppler shifts from rotation and expansion are important).

3. MODEL RESULTS

In this section we explore the combined effects of gravity darkening and limb darkening on the continuum polarization produced by circumstellar disks. We will consider two different geometries: a thin dense disk representative of Be star envelopes; and a moderately flattened envelope (thick disk) that has only a small density enhancement, such as may be present for rapidly rotating Wolf-Rayet or O stars.

3.1. *Equatorial Disks*

For this study we chose parameters in the density law to produce an equatorial disk with $\rho_{eq}/\rho_{pole} = 1000$, and an opening angle $\Delta\theta = 15°$ ($m = 20$). These are parameters commonly used to model the disks around Be stars (e.g., Waters 1986); however, combined observations of the IR excess and optical polarization indicate a disk opening angle of 0°.5 (Bjorkman 1992; see also Bjorkman & Cassinelli 1990). Theoretical predictions give opening angles in the range of 0°.5–3° (Bjorkman & Cassinelli 1992, 1993; Owocki, Cranmer, & Blondin 1994). Unfortunately, the parameter values associated with such a thin disk ($m = 500$ to 20,000) are computationally intractable using the present version of the polarization code.

To produce a Balmer jump in the polarization as large as that observed in ζ Tau requires an equatorial electron scattering optical depth $\tau_{es} \sim 1.5$. For our 15° disk at an inclination angle $i = 90°$, the polarization is about a factor of 2 higher than observed in ζ Tau (which is believed to be close to edge-on). This indicates that the disk is actually thinner than we have assumed here, because the polarization Balmer jump constrains the disk density, and the only other way to reduce the number of scatters is to make the disk thinner.

Figures 5–7 illustrate the effects of rotation rate on the UV continuum polarization of stars with different spectral types. The shape of the optical continuum is unaffected, except at late spectral types with very large rotation rates (see eq. [1]), so the only effect that gravity darkening has in the optical is to decrease the amplitude of the polarization. However, in going blueward from the Balmer jump, the UV continuum polarization begins to rise (due to the decrease in hydrogen bound-free absorption), reaches a maximum, and then begins to decrease, because the direct light from the star has a higher radiation temperature than the scattered light. Note that as the rotation rate increases, the temperature of the scattered light decreases, so the Wien peak of the scattered radiation occurs at longer wavelengths. Consequently, the UV polarization maximum shifts to larger wavelengths (see Fig. 7), and the amount of UV depolarization increases. This behavior offers a potential diagnostic that might be used to estimate the stellar rotation rate.

Figures 8 and 9 illustrate the effects of spectral type on the UV continuum polarization for rotating stars. Note that for nonrotating stars there is no spectral type dependence since we have not included the temperature dependence of the hydrogen ionization fraction. If we had included this dependence, the strength of the polarization Balmer jump and the slopes of the Balmer and Paschen continua would be a function of spectral type. For the rotating cases, large UV depolarization only occurs shortward of the Wien peak. This is why the peak of the UV polarization shifts to longer wavelengths and the depolarization is largest for later spectral types.

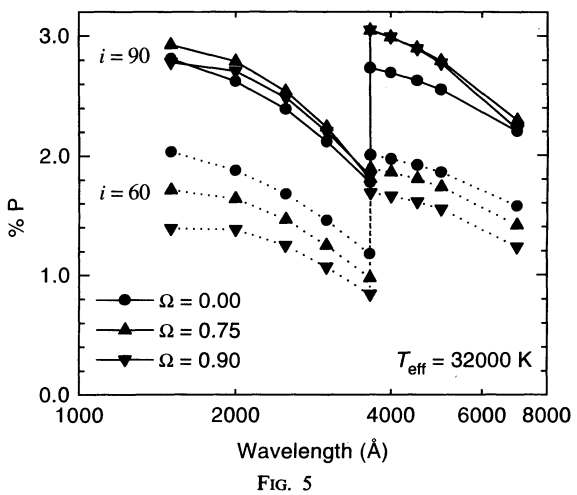

FIG. 5

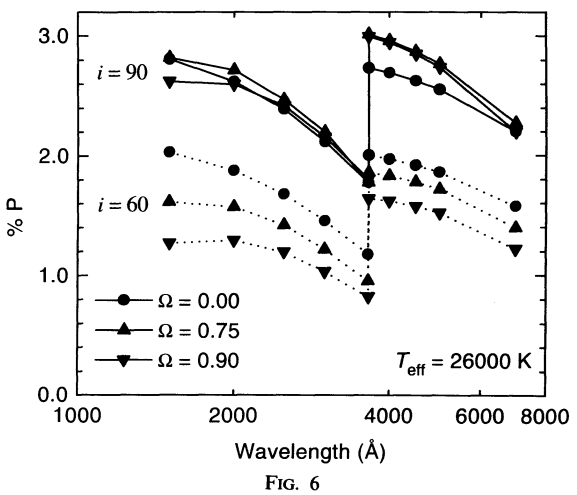

FIG. 6

FIG. 5.—Effects of gravity darkening on the polarization produced by the disk around a B0 Ve star as a function of rotation rate, $\Omega = V_{rot}/V_{crit}$, for two different inclination angles, i. Note that, for $i = 60°$ (*dotted curves*), the shape of each curve is the same in the optical and differs only in the UV.

FIG. 6.—Effects of gravity darkening on the polarization of a B1 Ve star as a function of rotation rate. Note that the UV depolarization is larger than that in Fig. 5.

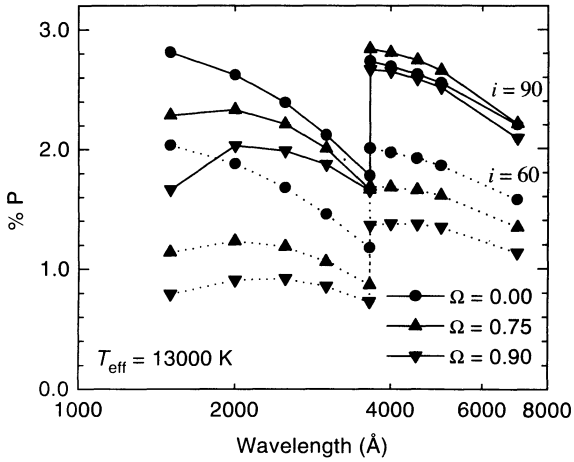

FIG. 7.—Effects of gravity darkening on the polarization of a B7 Ve star as a function of rotation rate. Note that there is a maximum in the UV polarization and that, as the rotation rate increases, the wavelength of the maximum increases. Also note that at a rotation rate of 90% break-up, the UV polarization is almost flat, but the gravity darkening is now beginning to affect the slope of the optical polarization as well.

For thin dense disks, the UV depolarization mechanism is dilution of the scattered light by direct radiation from the star that has a higher average temperature (see Fig. 2). If excessive limb darkening were the underlying cause of the temperature difference, then the amount of UV depolarization should be highly inclination angle dependent with little depolarization for edge-on cases. We have examined the model results for several inclination angles, and the curves have similar amounts of depolarization with only a small inclination angle dependence (compare the $i = 60°$ to the $i = 90°$ cases shown in Fig. 8). This implies that the predominant cause of the lower average radiation temperature seen by the scattering region is not limb darkening, but is instead occultation of the hot polar caps by the stellar limb.

3.2. *Flattened Envelopes*

For this study we chose parameters in the density law to produce an envelope with $\rho_{eq}/\rho_{pole} = 5$, a width $\Delta\theta = 33°$ ($m = 4$), and an equatorial optical depth $\tau_{es} \sim 0.5$, which produces a reasonable Balmer jump in the polarization. These are parameters that are appropriate for stars with large wind velocities, such as O stars, Wolf-Rayet stars, and some supergiants.

Figures 10 and 11 illustrate the effects of spectral type and rotation rate on the UV continuum polarization. The shape of the UV continuum polarization shown in Figure 10 is similar to that produced by thin dense disks, but the amount of UV depolarization is now much larger (cf. Fig. 6). Note that for the lowest temperature star shown in Figure 11, the polarization ($P = F_Q/F_I$) passes through zero and becomes negative at short wavelengths (actually the position angle "flips" by 90° and the magnitude of the polarization begins to increase). This indicates that the dominant UV depolarization mechanism for moderately flattened envelopes is *not* dilution by hotter direct light from the star, but instead is cancellation of the cooler polarized light scattered in the equator (which has $Q_v^{em} > 0$) by hotter polarized light scattered in the polar region (which has $Q_v^{em} < 0$). It is when the scattered polar flux exceeds the equatorial scattered flux that the polarization position angle flips 90°. Because the scattered flux depends not only on the

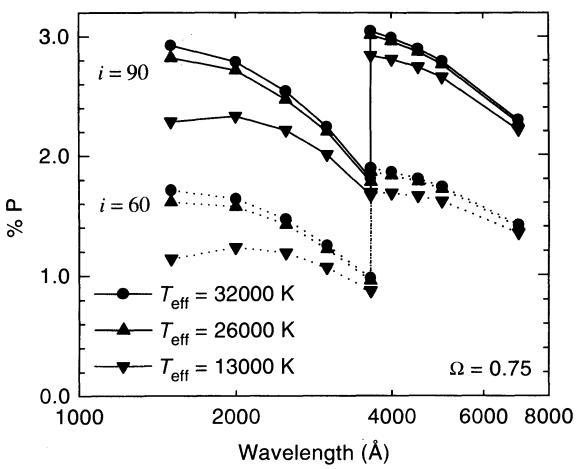

FIG. 8

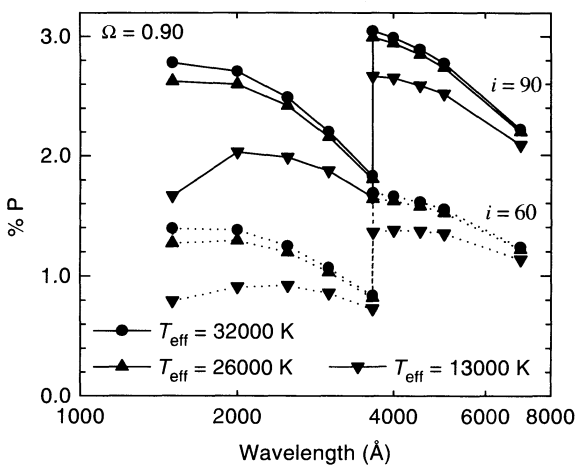

FIG. 9

FIG. 8.—Spectral type dependence of the polarization of a Be star rotating at 75% break-up. Note that large depolarization occurs only for the latest spectral type, since large depolarization only occurs for wavelengths that are shorter than the Wien peak of the stellar radiation.

FIG. 9.—Spectral type dependence of the polarization of a Be star rotating at 90% break-up. Again, large depolarization only occurs for the latest spectral type.

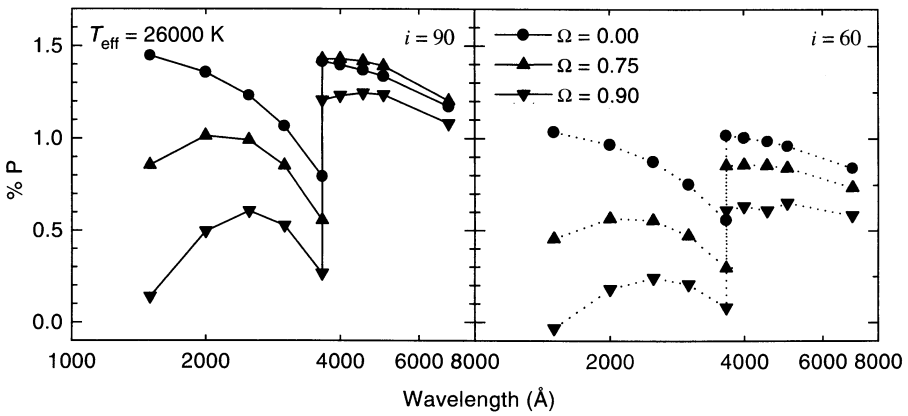

FIG. 10.—Effects of gravity darkening on the polarization produced by a B1 V star with an envelope that has $\rho_{eq}/\rho_{pole} = 5$, and an opening angle $\Delta\theta = 33°$ (i.e., only moderately flattened). The left panel shows the results for an inclination angle $i = 90°$, and the right panel is for $i = 60°$. Note that the UV depolarization is now much larger than before.

temperature of the scattered light, but also on the density of scatterers, the wavelength at which the position angle flips provides a potential diagnostic of the polar to disk density ratio, ρ_{eq}/ρ_{pole}.

4. DISCUSSION

We have seen that for a thin dense equatorial disk, the gravity darkening depolarization mechanism in the UV is dilution of the cool scattered light by hot direct radiation from the star. The dependence of the dilution on inclination angle of the observer is small, and in particular there is large depolarization even when $i = 90°$. If excessive limb darkening dominated, then the scattered radiation would have the same temperature as the direct radiation when $i = 90°$, and there would be no UV depolarization. Therefore, we infer that the underlying cause of the temperature difference is that, in the dominant scattering region of the disk, the stellar limb hides the hot stellar polar caps from the disk, so the disk only scatters the lower temperature radiation from the stellar equator.

On the other hand, for moderately flattened envelopes, the gravity darkening depolarization mechanism in the UV is cancellation of the cool (dim) equatorial polarization by hot (bright) polarized light that is scattered in the polar region. For small density contrasts between the pole and equator, this effect can be much larger than the dilution effect for thin disks. The signature of this situation is the 90° flip in the intrinsic position angle at short wavelengths.

A 90° position angle flip between the UV and optical polarization has been observed for the suspected Herbig Ae/Be star HD 45677 (Schulte-Ladbeck et al. 1992). However, in this case one may not conclude that gravity darkening is responsible, because there are at least three mechanisms that may cause the polar scattered radiation to be brighter than the equatorial scattered light: (1) a large ratio of polar to equatorial flux from the star (e.g., gravity darkening), (2) a wavelength dependent absorptive opacity that attenuates the equatorial radiation more than the polar radiation, such as an equatorially concentrated hydrogen bound-free opacity, and (3) a wavelength dependent scattering opacity, such as dust present in a circumstellar disk. Schulte-Ladbeck et al. (1992) conclude that the last mechanism (dust scattering) is the most likely explanation of the position angle flip of HD 45677.

In trying to explain the WUPPE observations of Be stars, gravity darkening can play a role. However, in the case of a thin dense disk, we see by comparing Figures 8 and 9 to Figure 1 that large UV depolarization requires a much cooler stellar temperature than

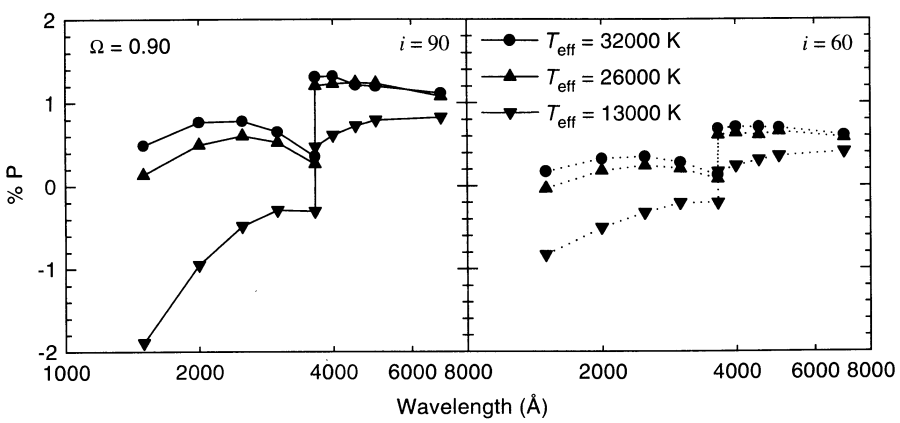

FIG. 11.—Spectral type dependence of the polarization of a moderately flattened envelope. The left panel shows the results for an inclination angle $i = 90°$, and the right panel is for $i = 60°$. Note that at late spectral types the polarization becomes negative (a 90° flip in position angle). This is because the scattered polar flux is brighter than the scattered equatorial flux.

indicated by the B1 spectral type of ζ Tau, and it also requires a rotation rate much larger than the observed $v \sin i = 220$ km $s^{-1} = 0.45 V_{crit}$. On the other hand in the case of a moderately flattened envelope, there can be large depolarization effects even for a B1 star (see Fig. 10); however, *the shape* of the UV continuum does not match the observed UV polarization (compare Fig. 10 with the data shown in Fig. 1). We conclude that gravity-darkening depolarization can at most only partially explain the discrepancy between the observations and previous theoretical models. This implies that there must be an additional depolarization mechanism. A likely source is metal line blanketing in the Balmer continuum (Bjorkman et al. 1991), and this mechanism is currently under investigation.

We wish to thank J. P. Cassinelli, J. C. Brown, and K. H. Nordsieck for many useful discussions on this topic. We also thank M. R. Meade and B. L. Babler for invaluable help with WUPPE and PBO data. This research has been supported by NASA grant NAGW-2921 and NASA contract NAS5-26777 to the University of Wisconsin.

REFERENCES

Bjorkman, J. E. 1992, Ph.D. thesis, Univ. Wisconsin
Bjorkman, J. E., & Cassinelli, J. P. 1990, in Angular Momentum and Mass Loss for Hot Stars, ed. L. A. Willson & R. Stalio (Dordrecht: Kluwer), 185
———. 1992, in ASP Conf. Ser. 22, Nonisotropic and Variable Outflows from Stars, ed. L. Drissen, C. Leitherer, & A. Nota (San Francisco: ASP), 88
———. 1993, ApJ, 409, 429
Bjorkman, K. S., et al. 1991, ApJ, 383, L67 (Paper I)
———. 1993, ApJ, 412, 810 (Paper II)
Brown, J. C., Carlaw, V. A., & Cassinelli, J. P. 1989, ApJ, 344, 341
Cassinelli, J. P., Nordsieck, K. H., & Murison, M. A. 1987, ApJ, 317, 290
Chandrasekhar, S. 1960, Radiative Transfer (New York: Dover)
Collins, G. W., II, 1970, ApJ, 159, 583
Collins, G. W., II, Truax, R. J., & Cranmer, S. R. 1991, ApJS, 77, 541
Coyne, G. V. 1976, in IAU Symp. 70, Be and Shell Stars, ed. A. Slettebak (Dordrecht: Reidel), 233
Fox, G. K. 1993, MNRAS, 260, 513
Friend, D. B., & Abbott, D. C. 1986, ApJ, 311, 701
Hillier, D. J. 1993, A&A, submitted
McLean, I. S., & Clarke, D. 1979, MNRAS, 186, 245
Mihalas, D. 1978, Stellar Atmospheres (San Francisco: Freeman)
Osterbrock, D. E. 1989, Astrophysics of Gaseous Nebulae and Active Galactic Nuclei (Mill Valley, CA: University Science Books)
Owocki, S. P., Cranmer, S. R., & Blondin, J. M. 1994, ApJ, 424, 887
Poeckert, R., & Marlborough, J. M. 1978, ApJS, 38, 229
Schulte-Ladbeck, R. E., et al. 1992, ApJ, 401, L105
Sobolev, V. V. 1963, A Treatise on Radiative Transfer, tr. S. I. Gaposchkin (Princeton: van Nostrand)
von Zeipel, H. 1924, MNRAS, 84, 665
Waters, L. B. F. M. 1986, A&A, 162, 121
———. 1994, in IAU Symp. 162, Pulsation, Rotation, and Mass Loss in Early-Type Stars, ed. L. A. Balona, H. F. Henrichs, & J.-M. LeContel (Dordrecht: Kluwer), in press
Wood, K., & Bjorkman, J. E. 1994, ApJ, submitted